

The Compact Central Object in Cas A: A Neutron Star with Hot Polar Caps or a Black Hole?

G. G. Pavlov¹, V. E. Zavlin², B. Aschenbach², J. Trümper², and D. Sanwal¹

ABSTRACT

The central pointlike X-ray source of the Cas A supernova remnant was discovered in the *Chandra* First Light Observation and found later in the archival *ROSAT* and *Einstein* images. The analysis of these data does not show statistically significant variability of the source. Because of the small number of photons detected, different spectral models can fit the observed spectrum. The power-law fit yields the photon index $\gamma = 2.6\text{--}4.1$, and luminosity $L(0.1\text{--}5.0\text{ keV}) = (2\text{--}60) \times 10^{34}\text{ erg s}^{-1}$, for $d = 3.4\text{ kpc}$. The power-law index is higher, and the luminosity lower, than those observed from very young pulsars. One can fit the spectrum equally well with a blackbody model with $T = 6\text{--}8\text{ MK}$, $R = 0.2\text{--}0.5\text{ km}$, $L_{\text{bol}} = (1.4\text{--}1.9) \times 10^{33}\text{ erg s}^{-1}$. The inferred radii are too small, and the temperatures too high, for the radiation could be interpreted as emitted from the whole surface of a uniformly heated neutron star. Fits with the neutron star atmosphere models increase the radius and reduce the temperature, but these parameters are still substantially different from those expected for a young neutron star. One cannot exclude, however, that the observed emission originates from hot spots on a cooler neutron star surface. Because of strong interstellar absorption, the possible low-temperature component gives a small contribution to the observed spectrum; an upper limit on the (gravitationally redshifted) surface temperature is $T_s^\infty < 1.9\text{--}2.3\text{ MK}$, depending on chemical composition of the surface and star's radius. Amongst several possible interpretations, we favor a model of a strongly magnetized neutron star with magnetically confined hydrogen or helium polar caps ($T_{\text{pc}}^\infty \approx 2.8\text{ MK}$, $R_{\text{pc}} \approx 1\text{ km}$) on a cooler iron surface ($T_s^\infty \approx 1.7\text{ MK}$). Such temperatures are consistent with the standard models of neutron star cooling. Alternatively, the observed radiation may be interpreted as emitted by a compact object (more likely, a black hole) accreting from a fossil disk or from a late-type dwarf in a close binary.

Subject headings: stars: neutron — supernovae: individual (Cas A) — X-rays: stars

¹ The Pennsylvania State University, 525 Davey Lab, University Park, PA 16802, USA; pavlov@astro.psu.edu

² Max-Planck-Institut für Extraterrestrische Physik, D-85740 Garching, Germany; zavlin@xray.mpe.mpg.de

1. Introduction

Cassiopeia A is the brightest shell-type galactic supernova remnant (SNR) in X-rays and radio, and the youngest SNR observed in our Galaxy. The radius of the approximately spherical shell is $\approx 2'$, which corresponds to ≈ 2 pc for the distance $d = 3.4_{-0.1}^{+0.3}$ kpc (Reed et al. 1995). The supernova which gave rise to Cas A was probably first observed in 1680 (Ashworth 1980). It is thought to be a Type II supernova caused by explosion of a very massive Wolf-Rayet star (Fesen, Becker & Blair 1987). Optical observations of Cas A show numerous oxygen-rich fast-moving knots (FMK), with velocities of about 5000 km s^{-1} , and slow-moving quasi-stationary flocculi, with typical velocities of about 200 km s^{-1} , which emit $\text{H}\alpha$ and strong lines of nitrogen. X-ray observations of Cas A show numerous clumps of hot matter emitting strong Si, S, Fe, Ar, Ne, Mg and Ca lines (Holt et al. 1994, and references therein). Because this SNR lies at the far side of the Perseus arm, with its patchy distribution of the interstellar gas, the interstellar absorption varies considerably across the Cas A image (e.g., Keohane, Rudnick & Anderson 1996). Numerous radio, optical and X-ray measurements of the hydrogen column density (e.g., Schwarz, Goss & Kalberla 1997; Hufford & Fesen 1996; Jansen et al. 1988; Favata et al. 1997) show a strong scatter within a range $0.5 \lesssim n_{H,22} \lesssim 1.6$, where $n_{H,22} \equiv n_H / (10^{22} \text{ cm}^{-2})$. Based on recent results, we consider $0.8 \lesssim n_{H,22} \lesssim 1.4$ as plausible values for the central region of the Cas A image.

In spite of considerable efforts to detect a compact remnant of the supernova explosion only upper limits on its flux had been established at different wavelengths until a pointlike X-ray source was discovered close to the Cas A center (Tananbaum et al. 1999) in the First Light Observation with the *Chandra* X-ray Observatory (see Weisskopf et al. 1996 for a description). After this discovery, the same source was found in the *ROSAT* HRI image of 1995–96 (Aschenbach 1999) and *Einstein* HRI images of 1979 and 1981 (Pavlov & Zavlin 1999).

In this Letter we present the first analysis on the central source spectrum observed with *Chandra* (§2), together with the analysis of the *ROSAT*, *Einstein*, and *ASCA* observations (§3). Various interpretations of these observations are discussed in §4.

2. *Chandra* ACIS observation and the point source spectrum

The SNR Cas A was observed several times during the *Chandra* Orbital Activation and Calibration Phase. For our analysis, we chose four observations of 1999 August 20–23 with the S array of the Advanced CCD Imaging Spectrometer (ACIS; Garmire 1997). In these observations Cas A was imaged on the backside-illuminated chip S3. The spectral response of this chip is presently known better than those of the frontside-illuminated chips used in a few other ACIS observations of Cas A. We used the processed data products available from the public *Chandra* Data Archive. The observations were performed in the Timed Exposure mode, with a frame integration time of 3.24 s. The durations of the observations were 5.03, 2.04, 1.76, and 1.77 ks. Because of telemetry saturation, the effective exposures were 2.81, 1.22, 1.06, and 1.05 ks,

respectively. Since the available ACIS response matrices were generated for the set of grades G02346, we selected events with these grades. Events with pulse height amplitudes exceeding 4095 ADU ($\approx 0.7\%$ of the total number) were discarded as generated by cosmic rays. The images of the pointlike source look slightly elongated, but this elongation is likely caused by errors in the aspect solution, and the overall shapes of the images is consistent with the assumption that this is a point source. Its positions in the four observations are consistent with that reported by Tananbaum et al. (1999): $\alpha_{2000} = 23^{\text{h}}23^{\text{m}}27^{\text{s}}.94$, $\delta_{2000} = +58^{\circ}48'42''.4$. For each of the images, we extracted the source+background counts from a $3''$ radius circle around the point source center, and the background from an elliptical region around the circle, with an area of about 10 times that of the circle. After subtracting the background, we obtained the source countrates 112 ± 8 , 121 ± 13 , 112 ± 14 , and 127 ± 15 ks^{-1} (counts per kilosecond). The countrate values and the light curves are consistent with the assumption that the source flux remained constant during the 4 days, with the countrate of 116 ± 6 ks^{-1} .

For the analysis of the point source spectrum, we chose the longest of the ACIS-S3 observations. We grouped the pulse-height spectrum for 306 source counts into 14 bins in the 0.8–5.0 keV range (Fig. 1). Each bin has more than 20 counts (except for the highest-energy bin with 8 counts). The spectral fits were performed with the XSPEC package.

If the source is an active pulsar, we can expect that its X-ray radiation is emitted by relativistic particles and has a power-law spectrum. The power-law fit (upper panel of Fig. 2) yields a photon index $\gamma = 3.2^{+0.9}_{-0.6}$ (all uncertainties are given at a $1\text{-}\sigma$ confidence level) that is considerably larger than $\gamma = 1.4\text{--}2.1$ observed for X-ray radiation from youngest pulsars (Becker & Trümper 1997). The hydrogen column density, $n_{H,22} = 1.7^{+0.7}_{-0.5}$, inferred from the power-law fit somewhat exceeds estimates obtained from independent measurements (see §1). The (unabsorbed) X-ray luminosity in the 0.1–5.0 keV range, $L_X = 5.8^{+58.3}_{-4.3} \times 10^{34} d_{3.4}^2$ erg s^{-1} , where $d_{3.4} = d/(3.4 \text{ kpc})$, is lower than those observed from very young pulsars (e.g., 1.5×10^{36} and 2.3×10^{36} erg s^{-1} for the Crab pulsar and PSR B0540–69, in the same energy range).

If the source is a neutron star (NS), but not an active pulsar, thermal radiation from the NS surface can be observed. The blackbody fit (middle panel of Fig. 2) yields a temperature $T_{\text{bb}}^{\infty} = 7.1^{+1.1}_{-1.0}$ MK and a sphere radius $R_{\text{bb}}^{\infty} = 0.29^{+0.16}_{-0.09} d_{3.4}$ km, which correspond to a bolometric luminosity $L_{\text{bb,bol}}^{\infty} = 1.6^{+0.3}_{-0.2} \times 10^{33} d_{3.4}^2$ erg s^{-1} . (We use the superscript ∞ to denote the observed quantities, distinguishing them from those at the NS surface: $T^{\infty} = g_r T$, $L^{\infty} = g_r^2 L$, $R^{\infty} = g_r^{-1} R$, where $g_r = [1 - 2GM/Rc^2]^{1/2} = [1 - 0.41M_{1.4}R_6^{-1}]^{1/2}$ is the gravitational redshift factor, $M = 1.4M_{1.4}M_{\odot}$ and $R = 10^6 R_6$ cm are the NS mass and radius). The temperature is too high, and the radius is too small, to interpret the detected X-rays as emitted from the whole surface of a cooling NS with a uniform temperature distribution. The inferred hydrogen column density, $n_{H,22} = 0.6^{+0.5}_{-0.3}$, is on a lower side of the plausible n_H range.

Since fitting observed X-ray spectra with light-element NS atmosphere models yields lower effective temperatures and larger emitting areas (e. g., Zavlin, Pavlov & Trümper 1998), we fit

the spectrum with a number of hydrogen and helium NS atmosphere models (Pavlov et al. 1995; Zavlin, Pavlov & Shibano 1996), for several values of NS magnetic field. These fits show that the assumption that the observed radiation is emitted from the whole surface of a 10-km radius NS with a uniform temperature still leads to unrealistically large distances, $\sim 20\text{--}50$ kpc. Thus, both the blackbody fit and H/He atmosphere fits hint that, if the object is a NS, the observed radiation emerges from hot spots on its surface (see §4). An example of such a fit, for polar caps covered with a hydrogen atmosphere with $B = 5 \times 10^{12}$ G, is shown in the bottom panel of Figure 2. The model spectra used in this fit were obtained assuming the NS to be an orthogonal rotator (the angles α , between the magnetic and rotation axes, and ζ , between the rotation axis and line of sight, equal 90°). The inferred effective temperature of the caps is $T_{\text{pc}} = 5.9_{-1.6}^{+1.4}$ MK (which corresponds to $T_{\text{pc}}^\infty = 4.5_{-1.2}^{+1.1}$ MK), the polar cap radius $R_{\text{pc}} = 0.8_{-0.3}^{+1.1} d_{3.4}$ km, and $n_{H,22} = 0.7_{-0.3}^{+0.4}$. The bolometric luminosity of two polar caps is $L_{\text{pc,bol}} = 2.6_{-0.5}^{+1.7} \times 10^{33} d_{3.4}^2 \text{ erg s}^{-1}$. The temperature T_{pc} can be lowered, and the polar cap radius increased, if we see the spot face-on during the most part of the period — extreme values, $T_{\text{pc}} = 3.8_{-0.8}^{+1.1}$ MK ($T_{\text{pc}}^\infty = 2.9_{-0.5}^{+0.8}$ MK) and $R_{\text{pc}} = 0.9_{-0.3}^{+1.2} d_{3.4}$ km, at $n_{H,22} = 0.8_{-0.4}^{+0.5}$, correspond to $\alpha = \zeta = 0$.

The fits with the one-component thermal models implicitly assume that the temperature of the rest of the NS surface is so low that its radiation is not seen by ACIS. On the other hand, according to the NS cooling models (e.g., Tsuruta 1998), one should expect that, at the age of 320 yr, the (redshifted) surface temperature can be as high as 2 MK for the so-called standard cooling (and much lower, down to 0.3 MK, for accelerated cooling). To constrain the temperature outside the polar caps, we repeated the polar cap fits with the second thermal component added, at a fixed NS radius and different (fixed) values of surface temperature T_s . With this approach we estimated upper limits on the lower temperature, $T_s^\infty < 1.9\text{--}2.3$ MK (at a 99% confidence level), depending on the low-temperature model chosen. These fits show that the model parameters are strongly correlated — the increase of T_s shifts the best-fit T_{pc} downward, and n_H upward. For example, using an iron atmosphere model for the low-temperature component and assuming a hydrogen polar cap, we obtain an acceptable fit (see Fig. 1) for $T_s^\infty = 1.7$ MK, $R = 10$ km, $T_{\text{pc}}^\infty = 2.8$ MK, $R_{\text{pc}} = 1.0 d_{3.4}$ km, $n_{H,22} = 1.1$. Note that this T_s is consistent with the predictions of the standard cooling models, and n_H is close to most plausible values adopted for the central region of the SNR.

3. Analysis of the *ROSAT*, *Einstein* and *ASCA* images

We reanalyzed the archival data on Cas A obtained during a long *ROSAT* HRI observation, between 1995 December 23 and 1996 February 1 (dead-time corrected exposure 175.6 ks). The image shows a pointlike central source at the position $\alpha_{2000} = 23^{\text{h}}23^{\text{m}}27^{\text{s}}.57$, $\delta_{2000} = 58^\circ48'44''.0$ (coordinates of the center of the brightest $0''.5 \times 0''.5$ pixel), consistent with that reported by Aschenbach (1999). Its separation from the *Chandra* point source position, $3''.3$, is smaller than the *ROSAT* absolute pointing uncertainty (about $6''$; Briel et al. 1997). Measuring the source

countrate is complicated by the spatially nonuniform background. Another complication is that the 40-day-long exposure actually consists of many single exposures of very different durations. Because of the absolute pointing errors, combining many single images in one leads to additional broadening of the point source function (PSF). To account for these complications, we used several apertures (with radii from $3''$ to $7''$) for source+background extraction, measured background in several regions with visually the same intensity as around the source, discarded short single exposures, and used various combinations of long single exposures for countrate calculations. This analysis yields a source countrate of $4.6 \pm 0.8 \text{ ks}^{-1}$ (corrected for the finite apertures).

We also re-investigated the archival data on Cas A obtained with the *Einstein* HRI in observations of 1979 February 8 (42.5 ks exposure) and 1981 January 22–23 (25.6 ks exposure). In each of the data sets there is a pointlike source at the positions $\alpha_{2000} = 23^{\text{h}}23^{\text{m}}27^{\text{s}}.83$, $\delta_{2000} = 58^{\circ}48'43''.9$, and $\alpha_{2000} = 23^{\text{h}}23^{\text{m}}27^{\text{s}}.89$, $\delta_{2000} = 58^{\circ}48'43''.7$, respectively, consistent with those reported by Pavlov & Zavlin (1999). The separations from the *Chandra* position, $1''.7$ and $1''.4$, and from the *ROSAT* position, $2''.0$ and $2''.5$, are smaller than the nominal absolute position uncertainty ($\sim 4''$ for *Einstein*). Since the observations were short, estimating the source counrates is less complicated than for the *ROSAT* HRI observation. The source+background counts were selected from $5''$ -radius circles, and the background was measured from annuli of $10''$ outer radii surrounding the circles. The source counrates, calculated with account for the HRI PSF (Harris et al. 1984), are 2.2 ± 0.5 (Feb 1979), $2.7 \pm 0.8 \text{ ks}^{-1}$ (Jan 1981), and $2.4 \pm 0.6 \text{ ks}^{-1}$ (for the combined data). The countrate is consistent with the upper limit of 7.5 ks^{-1} , derived by Murray et al. (1979) from the longer of the two observations.

To check whether the source radiation varied during the two decades, we plotted the lines of constant *ROSAT* and *Einstein* HRI counrates in Figure 2. For all the three one-component models, the domains of model parameters corresponding to the *Einstein* HRI counrates within a $\pm 1\sigma$ range are broader than the 99% confidence domains obtained from the *Chandra* spectra. The $1\text{-}\sigma$ domains corresponding to the *ROSAT* HRI countrate overlap with the $1\text{-}\sigma$ confidence regions obtained from the spectral data. Thus, the source counrates detected with the three instruments do not show statistically significant variability of the source.

We also examined numerous archival *ASCA* observations of Cas A (1993–1999) and failed to detect the central point source on the high background produced by bright SNR structures smeared by poor angular resolution of the *ASCA* telescopes. In the longest of the *ASCA* SIS observations (1994 July 29; 15.1 ks exposure) the point source would be detected at a $3\text{-}\sigma$ level if its flux were a factor of 8 higher than that observed with *Chandra*, *ROSAT*, and *Einstein*. The *ASCA* observations show that there were no strong outbursts of the central source.

4. Discussion

The observed X-ray energy flux, F_X , of the compact central object (CCO³) is 3.6, 6.5, and 8.2×10^{-13} erg cm⁻² s⁻¹ in 0.3–2.4, 0.3–4.0 and 0.3–6.0 keV ranges, respectively. Upper limits on its optical-IR fluxes, $F_R \lesssim 3 \times 10^{-15}$ erg cm⁻² s⁻¹ and $F_I \lesssim 1 \times 10^{-14}$ erg cm⁻² s⁻¹, can be estimated from the magnitude limits, $R \gtrsim 24.8$ and $I \gtrsim 23.5$, found by van den Bergh & Pritchett (1986). This gives, e.g., $F_X/F_R \gtrsim 100$ for the *ROSAT* energy range, and $F_X/F_R \gtrsim 200$ for the *Chandra* and *Einstein* ranges. The flux ratios are high enough to exclude coronal emission from a noncompact star as the source of the observed X-ray radiation. A hypothesis that CCO is a background AGN or a cataclysmic variable cannot be completely rejected, but its probability looks extremely low, given the high X-ray-to-optical flux ratio, the softness of the spectrum, and the lack of indications on variability.

The strong argument for CCO to be a compact remnant of the Cas A explosion is its proximity to the Cas A center. In particular, this source lies 7''–11'' south of the SNR geometrical center determined from the radio image of Cas A (see Reed et al. 1995, and references therein). The source separation, 1''–5'', from the SNR expansion center, found by van den Bergh & Kamper (1983) from the analysis of proper motions of FMKs, corresponds to a transverse velocity of 50–250 km s⁻¹ (for $d = 3.4$ kpc, $\tau = 320$ yr). Much higher transverse velocities, 800–1000 km s⁻¹, correspond to the separation, 16''–20'', from the position of the apparent center of expanding SNR shell derived by Reed et al. (1995) from the radial velocities of FMKs. Thus, if CCO is the compact remnant of the SN explosion, it is moving south (or SSE) from the Cas A center with a transverse velocity of a few hundred km s⁻¹, common for radio pulsars.

If CCO is an isolated (nonaccreting) object, it might be an active pulsar with an unfavorable orientation of the radio beam (a limit on the pulsed flux of 80 mJy at 408 MHz was reported by Woan & Duffett-Smith 1993). However, a lack of a plerion or a resolved synchrotron nebula, together with the steep X-ray spectrum and low luminosity (see §2) do not support this hypothesis. The lack of the pulsar activity has been found in several X-ray sources associated with young compact remnants of SN explosions (e.g., Gotthelf, Vasisht & Dotani 1999); it may be tentatively explained by superstrong ($\gtrsim 10^{14}$ G) magnetic fields which may suppress the one-photon pair creation in the pulsar's acceleration gaps (Baring & Harding 1998).

If CCO is an isolated NS without pulsar activity, one may assume that the observed X-rays are emitted from the NS surface. In this case, we also have to assume an intrinsically nonuniform surface temperature distribution to explain the small size and high temperature of the emission region. Slight nonuniformity of the surface temperature can be caused by anisotropy of heat conduction in the strongly magnetized NS crust (Greenstein & Hartke 1983). However, this nonuniformity is not strong enough to explain the small apparent areas of the emitting regions.

³According to the convention recommended by the *Chandra* Science Center, this source should be named CXO J232327.9+584842. We use the abbreviation CCO for brevity.

Some nonuniformity might be expected in magnetars, if they are indeed powered by decay of their superstrong magnetic fields (Thompson & Duncan 1996; Heyl & Kulkarni 1998) and a substantial fraction of the thermal energy is produced in the outer NS crust. In this case, the hotter regions of the NS surface would be those with stronger magnetic fields. If additional investigations will demonstrate quantitatively that the observed luminosity of $\sim 10^{33}$ erg s $^{-1}$ can be emitted from a small fraction, $\sim 10^{-2}$, of the magnetar’s surface, we should expect that the radiation is pulsed, with a probable period of a few seconds typical for magnetars. We can also speculate that CCO is a predecessor of a soft gamma-repeater (such a hypothesis has been proposed by Gotthelf et al. 1999 for the central source of the Kes 73, which shows a spectrum similar to CCO, albeit emitted from a larger area).

Higher temperatures of polar caps can be explained by different chemical compositions of the caps and the rest of the NS surface. Light-element polar caps could form just after the SN explosion via fallback of a fraction of the ejected matter onto the magnetic poles. Due to fast stratification in the strong gravitational field, the upper layers of the polar caps will be comprised of the lightest element present. The thermal conductivity in the liquid portion of thin degenerate NS envelopes, which is responsible for the temperature drop from the nearly isothermal interior to the surface, is proportional to Z^{-1} , where Z is the ion charge (Yakovlev & Urpin 1980). This means that low- Z envelopes are more efficient heat conductors than high- Z ones, so that a light-element (H, He) surface has a higher effective temperature for a given temperature T_b at the outer boundary of the internal isothermal region. Approximately, the effective surface temperature is proportional to $Z^{-1/4}$ if the chemical composition of the envelope does not vary with depth, so that the surface of a hydrogen envelope can be 2.2 times hotter than that of an iron envelope. Numerical calculations of Chabrier, Potekhin & Yakovlev (1997) give a smaller factor (1.6–1.7 for temperatures of interest), with account for burning of light elements into heavier ones in the hot bottom layers of the envelope, but neglecting the effects of strong magnetic fields which can somewhat increase this factor (Heyl & Hernquist 1997). Hence, the light-element cap should be hotter than the rest of the NS surface. For instance, for $T_b = 400$ MK, the effective temperatures of the H cap and Fe surface are $T_{\text{pc}}^\infty = 2.8$ MK and $T_s^\infty = 1.7$ MK, for $M = 1.4M_\odot$, $R = 10$ km. As we have shown in §2, a two-component model spectrum with such temperatures is consistent with the observed CCO spectrum, for $R_{\text{pc}} \simeq 1$ km. The thickness of the hydrogen cap, $\gtrsim 2 \times 10^{13}$ g cm $^{-2}$, needed to provide such a temperature difference, corresponds to the total cap mass $M_{\text{pc}} \sim 6 \times 10^{23} (R_{\text{pc}}/1 \text{ km})^2$ g. For lower M_{pc} , the temperature difference will be smaller, but still appreciable for $M_{\text{pc}} \gtrsim 10^{-12} M_\odot$. Such an explanation of the CCO radiation is compatible only with the standard cooling scenario — the difference of chemical compositions could not account for a large ratio, ~ 10 , of the cap and surface temperatures required by the accelerated cooling.

Let us consider the hypothesis that the observed X-ray radiation is due to accretion onto a NS or a black hole (BH). To provide a luminosity $L = L_{33} \times 10^{33}$ erg s $^{-1}$, the accretion rate should be $\dot{M} = L/(\xi c^2) = 1.1 \times 10^{12} L_{33} \xi^{-1}$ g s $^{-1}$, where ξ is the accretion efficiency ($\xi = 0.2 M_{1.4} R_6^{-1}$ for accretion onto the surface of a NS). Although the luminosity and the accretion rate are

very small compared to typical values observed in accreting binaries, they are too high to be explained by accretion from circumstellar matter (CSM) — very high CSM densities and/or low object velocities relative to the accreting medium are required. For instance, the Bondi formula, $\dot{M} = 4\pi G^2 M^2 \rho v^{-3}$, gives the following relation between the CSM baryon density n and velocity $v = 100v_{100}$ km s⁻¹: $n = 8 \times 10^3 v_{100}^3 (0.2/\xi) M_{1.4}^{-2} L_{33}$ cm⁻³. Even at $v_{100} = 1$, which is lower than a typical pulsar velocity, the required density exceeds that expected in the Cas A interiors by about 3–4 orders of magnitude, unless the NS or BH moves within a much denser (and sufficiently cold) CSM concentration. This estimate for n can be considered as a lower limit because accretion onto a BH, or onto a NS in the propeller regime, is much less efficient.

We cannot, however, exclude that CCO is accreting from a secondary component in a close binary or from a fossil disk which remained after the SN explosion. We can rule out a massive secondary component — from the above-mentioned R and I limits, we estimate $M_R \gtrsim +8$, $M_I \gtrsim +8$. We can also exclude a persistent low-mass X-ray binary (LMXB) or a transient LMXB in outburst — the object would have a much higher X-ray luminosity than observed, and the accretion disk would be much brighter in the IR-optical range (van Paradijs & McClintock 1995). However, CCO might be a compact object with a fossil disk, or an LMXB with a dwarf secondary component, in a long-lasting quiescent state (e.g., an M5 dwarf with $M_{\text{bol}} = +9.8$ would have $I \simeq 24.7$, for the adopted distance and extinction). An indirect indication that CCO could be a compact accreting object is that its luminosity and spectrum resemble those of LMXBs in quiescence, although we have not seen variability inherent to such objects. If the accreting object were a young NS, it would be hard to explain how the matter accretes onto the NS surface — a very low magnetic field and/or long rotation period, $P \gtrsim 10^2 B_{12}^{6/7} L_{33}^{-3/7} R_6^{15/7} M_{1.4}^{-2/7}$ s, would be required for the accreting matter to penetrate the centrifugal barrier. The criterion suggested by Rutledge et al. (1999) to distinguish between the NS and BH LMXBs in quiescence, based on fitting the quiescent spectra with the light-element NS atmosphere models, favors the BH interpretation, although the applicability of this criterion to a system much younger than classical LMXBs may be questioned. On the other hand, in at least some of BH binaries optical radiation emitted by the accretion flow was detected in quiescence (e.g., Narayan, Barret & McClintock 1997) at a level exceeding the upper limit on the CCO optical flux. Finally, one could speculate that the CCO progenitor was a binary with an old NS, and this old NS has sufficiently slow rotation and low magnetic field to permit accretion onto the NS surface from a disk of matter captured in the aftermath of the SN explosion. In this case, CCO could have properties of an accreting X-ray pulsar with a low accretion rate. (A similar model was proposed by Popov 1998 for the central source of RCW 103, although he assumed accretion from the ISM.)

To conclude, we cannot firmly establish the nature of CCO based on the data available — it can be either an isolated NS with hot spots or a compact object (more likely, a BH) accreting from a fossil disk or from a dwarf binary companion. Although the CCO spectrum and luminosity strongly resemble those of other radio-quiet compact sources in SNRs, these sources may not necessarily represent a homogeneous group — e.g., the central source of Kes 73 shows 11.7 s

pulsations and remarkable stability, and was proposed to be a magnetar (Gotthelf et al. 1999), whereas the central source of RCW 103 shows long-term variability and no pulsations (Gotthelf, Petre & Vasisht 1999). We favor the isolated NS interpretation of CCO because it has not displayed any variability. Critical observations to elucidate its nature include searching for periodic and aperiodic variabilities, deep IR imaging, and longer *Chandra* ACIS observations which would provide more source quanta for the spectral analysis.

We are grateful to Norbert Schulz for providing the ACIS response matrices, to Gordon Garmire, Leisa Townsley and George Chartas for their advices on the ACIS data reduction, and to Niel Brandt, Sergei Popov, and Jeremy Heyl for useful discussions. The *ROSAT* and *Einstein* data were obtained through the High Energy Astrophysics Science Archive Research Center Online Service, provided by the NASA’s Goddard Space Flight Center. The work was partially supported through NASA grants NAG5-6907 and NAG5-7017.

REFERENCES

- Aschenbach, B. 1999, IAUC 7249
- Ashworth, W. B. 1980, *J. Hist. Astr.*, 11, 1
- Baring, M. G., & Harding, A. K. 1998, *ApJ*, 507, L55
- Becker, W., Trümper, J., 1997, *A&A*, 326, 682
- Briel, U. G., et al. 1997, “The *ROSAT* User’s Handbook”, MPE *ROSAT* Science Data Center, Garching (<http://wave.xray.mpe.mpg.de/rosat/doc/ruh>)
- Chabrier, G., Potekhin, A. Y., Yakovlev, D. G. 1997, *ApJ*, 477, L99
- Favata, F., et al. 1997, *A&A*, 324, L49
- Fesen, R. A., Becker, R. H., & Blair, W. P. 1987, *ApJ*, 313, 378
- Garmire, G. P. 1997, *BAAS*, AAS Mtg #190, #34.04
- Gotthelf, E. V., Petre, R., & Vasisht, G. 1999, *ApJ*, 514, L107
- Gotthelf, E. V., Vasisht, G., & Dotani, T. 1999, *ApJ*, 522, L49
- Greenstein, G., & Hartke, G. G. 1983, *ApJ*, 271, 283
- Harris, D. E., et al. 1984, *Einstein Observatory Revised User’s Manual*, Harvard-Smithsonian Center for Astrophysics
- Heyl, J. S., & Kulkarni, S. 1998, *ApJ*, 506, L61

- Heyl, J. S., & Hernquist, L. 1997, *ApJ*, 489, L67
- Holt, S. S., Gotthelf, E. V., Tsunemi, H., & Negoro, H. 1994, *PASJ*, 46, L151
- Hufford, A. P., & Fesen, R. A. 1996, *ApJ*, 469, 246
- Jansen, F., et al. 1988, *ApJ*, 331, 949
- Keohane, J. W., Rudnick, L., & Anderson, M. C. 1996, *ApJ*, 466, 309
- Murray, S. S., Fabbiano, G., Fabian, A. C., Epstein, A., & Giacconi, R. 1979, *ApJ*, 234, L69
- Narayan, R., Barret, D., & McClintock, J. E. 1997, *ApJ*, 482, 448
- Pavlov, G. G., & Zavlin, V. E. 1999, *IAUC* 7270
- Pavlov, G. G., Shibanov, Yu. A., Zavlin, V. E., & Meyer, R. D. 1995, in *The Lives of the Neutron Stars*, eds. M. A. Alpar, Ü. Kiziloğlu & J. van Paradijs (Kluwer: Dordrecht), p. 71
- Popov, S.B. 1998, *A&Ap Trans.*, 17, 35 (astro-ph/9708044; astro-ph/9806354)
- Reed, J. E., Hester, J. J., Fabian, A. C., & Winkler, P. F. 1995, *ApJ*, 440, 706
- Rutledge, R. E., Bildsten, L., Brown, E. F., Pavlov, G. G., & Zavlin, V. E. 1999, *ApJ*, in press (astro-ph/9909319)
- Schwarz, U. J., Goss, W. M., & Kalberla, P. M. V. 1997, *A&ASS*, 123, 43
- Tananbaum, H. 1999, *IAUC* 7246
- Thompson, C., & Duncan, R. C. 1996, *ApJ*, 473, 322
- Tsuruta, S. 1998, *Phys. Rep.*, 292, 1
- van den Bergh, S., & Kamper, K. W. 1983, *ApJ*, 268, 129
- van den Bergh, S., & Pritchett, C. J. 1986, *ApJ*, 307, 723
- van Paradijs, J., & McClintock, J. E. 1995, in *X-Ray Binaries*, Eds. W. H. G. Lewin, J. van Paradijs, & E. P. J. van den Heuvel (Cambridge Univ. Press: Cambridge), p.58
- Weisskopf, M. C., O'Dell, S. L., & Van Speybroeck, L. P. 1996, *Proc. SPIE* 2805, 2
- Woan, G., & Duffett-Smith, P. J. 1993, *MNRAS*, 260, 693
- Yakovlev, D. G., & Urpin, V. A. 1980, *Sov. Astr.*, 24, 303
- Zavlin, V. E., Pavlov, G. G., & Shibanov, Yu. A. 1996, *A&A* 315, 141
- Zavlin, V. E., Pavlov, G. G., & Trümper, J. 1998, *A&A*, 331, 821

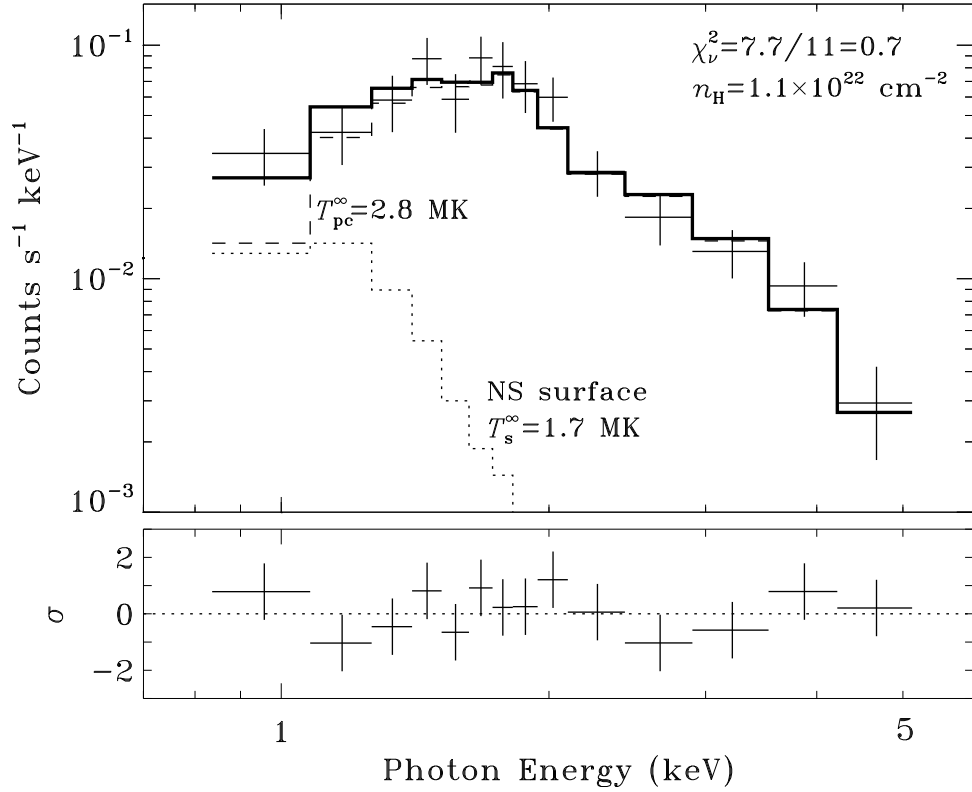


Fig. 1.— *Chandra* ACIS-S3 countrate spectrum from the central compact object of Cas A. The fit for hydrogen polar caps ($T_{\text{pc}}^\infty = 2.8 \text{ MK}$, $R_{\text{pc}} = 1 \text{ km}$) on a cooler iron NS surface ($T_{\text{s}}^\infty = 1.7 \text{ MK}$, $R = 10 \text{ km}$) is shown.

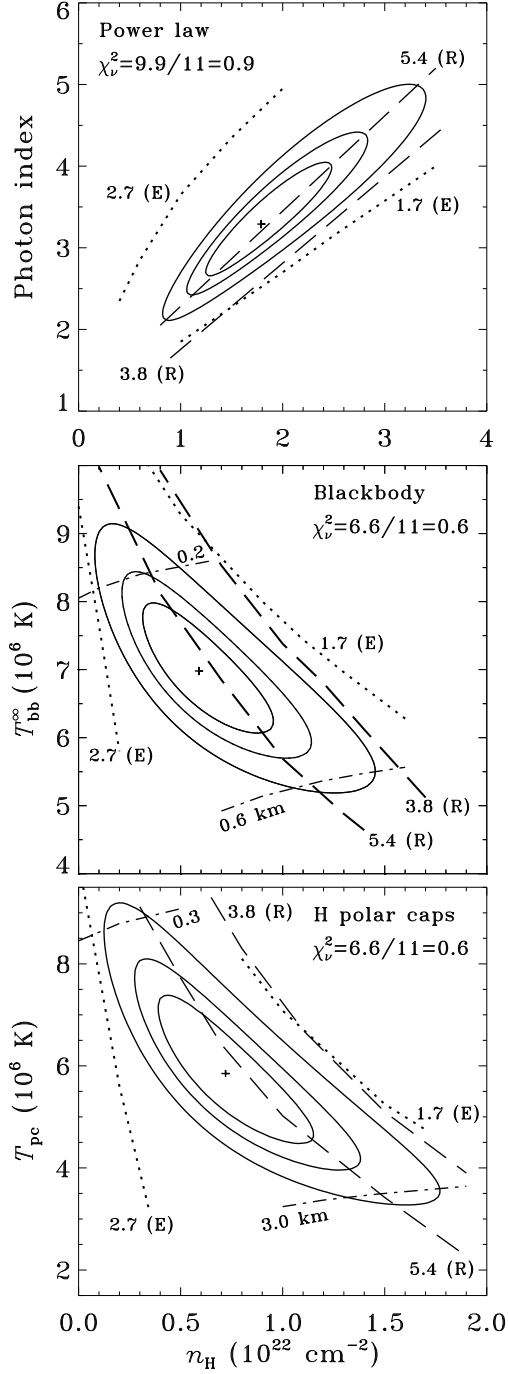


Fig. 2.— 67%, 90% and 99% confidence regions obtained from the fits to the spectrum of Figure 1, together with lines of constant *ROSAT* HRI (long dashes) and *Einstein* HRI (dots) countrates, in counts per kilosecond. The dash-dot curves in the two lower panels are the lines of constant radii of emitting areas (in km).